

The preparation, load and photocatalytic performance of N-doped and CdS-coupled TiO₂

Cite this: *RSC Advances*, 2013, 3, 9483

Mengmeng Liu,^a Jingtang Zheng,^{*a} Qian Liu,^b Shaojun Xu,^b Mingbo Wu,^b Qingzhong Xue,^b Zifeng Yan,^b Huiji Xiao,^c Zhenxing Wei^c and Haiyun Zhu^c

Various combinations of N-doped and CdS-coupled TiO₂ photocatalysts were studied for MO (methyl orange) degradation under visible light. The photodegradation of MO showed that CdS/N-TiO₂ was extremely sensitive to visible light and exhibited much higher activity than N-TiO₂ and CdS/TiO₂. The results indicated that the semiconductor coupled and N-doped modifications could enhance the photocatalytic performance. The absorption wavelength of CdS/N-TiO₂ was extended to 630 nm. The photocatalyst was then loaded on the Activated Carbon Fibers (ACFs) which could be activated by water vapor at 800 °C. In addition, the photodegradation rate of cyclic usage of the photocatalysts was also confirmed. The degradation efficiency of methyl orange with CdS/N-TiO₂/ACFs was markedly higher than for the ACF and CdS/TiO₂/ACFs composites. The photocatalysts were tightly bound to the ACFs and could be easily handled and recovered from water. At the same time, loading the photocatalysts onto the ACFs could reduce Cd²⁺ leaching efficiently, from 38% to 7% approximately.

Received 20th January 2013,
Accepted 5th April 2013

DOI: 10.1039/c3ra40288f

www.rsc.org/advances

Introduction

Photocatalysis has attracted considerable scientific interest owing to its potential application in purification. TiO₂ is most widely used as a semiconductor photocatalyst for the effective decomposition of organic compounds in air and water under UV light irradiation, with a wavelength shorter than 387 nm.^{1,2} However, its wide band gap (3.2 eV) has restricted its practical application. Up to now various methods have been developed to extend the light absorbance into the visible light region and thus improve the photocatalytic efficiency, such as doping with other impurities, depositing noble metals on TiO₂ and combining TiO₂ with other semiconductors.^{3,4}

Many previous studies indicated that doping TiO₂ with nitrogen was one of the most effective approaches in improving the properties and photocatalytic activity of TiO₂ in the visible light region.^{5,6} Nitrogen could be incorporated into the TiO₂ structure as substitutional and interstitial. The introduction of substitutional N atoms into the TiO₂ matrix improves optical absorption in the visible region, and leads to corresponding photochemical activity.^{7,8} The nitrogen doping has predominant effects on the improvement of the photocatalytic activity: on one hand, it can narrow the band gap of

titania to extend its absorption to the visible light region; on the other hand, it can increase the separation efficiency of the photo induced electron and hole.⁷ Moreover, CdS is a semiconductor with a band gap of 2.4 eV and is considered to be one of the many sensitizers used for large band gap semiconductors because of the ideal position of its conduction and valence band edges.⁹ CdS alone, however, shows negligible photocatalytic activity because of its instability and rapid electron-hole pair recombination rates. Studies have reported that with the appropriate particle interaction, CdS/TiO₂ can efficiently decompose organic compounds such as phenol and methylene blue under visible light irradiation of less than 495 nm.¹⁰⁻¹² Q. Zhang, J. Sun, *et al.*, assembled a PbSe and CdS nanoparticle (NP) co-sensitized nitrogen-doped TiO₂ nanorod array which enhanced the photocurrent and had better photoelectrochemical (PEC) performance.¹³ As we know, both N-doped TiO₂ or CdS-coupled TiO₂ can extend the visible light region, but it is not known how they work when the two methods are combined together, especially whether they could have a better photoresponse to visible light and improve the photoactivity. However, as with other powder photocatalysts and nanoparticles, they have some disadvantages, such as difficult recovery, easy cohesion and low utilization rate in practical applications. An alternative method is immobilizing nanoparticles onto an inert and porous supporting matrix; through the accumulation of carriers the adsorption mass transfer rate and efficiency of the photocatalytic degradation are effectively improved.¹⁴⁻¹⁷ Activated carbon fiber (ACF) is a newly developed type of photocatalyst support material with larger pore volume and more uniform micropore size

^aState Key Laboratory of Heavy Oil Processing, College of Chemical Engineering, China University of Petroleum, Qingdao, Shandong 266580, P. R. China.

E-mail: jtzheng03@163.com; Fax: (+)86 546 8395190; Tel: 13854628317

^bCollege of Chemical Engineering, China University of Petroleum (East China), Qingdao 266580, P. R. China

^cState Key Laboratory of Heavy Oil Processing, College of Science, China University of Petroleum, Qingdao, Shandong 266580, P. R. China

distribution.^{18–20} In addition, ACFs can relieve the pollution of Cd^{2+} produced by the photocorrosion of CdS. The results presented in this study will make significant contributions towards the development of delicate composite photocatalysts for photocatalytic water purification and solar energy utilization.

In this work, two or more modification technologies were used to modify TiO_2 . The photocatalysts prepared not only reduced the charge carrier but also enhanced the range of the spectrum. We attempted to immobilize the photocatalysts on the surface of ACF *via* adhesion. The aims of our study were: (1) to synthesize N-doped and CdS-coupled TiO_2 by a sol-gel method; (2) to access the photocatalytic and photophysical properties of photocatalysts and composites with ACFs; (3) to explore the reuse of the photocatalyst/ACF composites in order to realize cyclic photodegradation; (4) to study if ACFs could prevent Cd^{2+} ions from leaching.

Experimental

2.1 Materials

All reagents used were of analytical grade and were employed as received. Activated carbon fibers (ACFs, specific surface area of $1150\text{--}1250\text{ m}^2\text{ g}^{-1}$), tetrabutyl titanate (TBOT), acetic acid (CH_3COOH), methyl orange (MO), ammonium chloride (NH_4Cl), ammonium hydroxide solution (NH_4OH), cadmium acetate ($\text{Cd}(\text{Ac})_2 \cdot 2\text{H}_2\text{O}$), thiourea ($\text{SC}(\text{NH}_2)_2$) and epoxy resin were purchased from Tianjin, China. Water used for solution and experimental preparations was ultrapure.

2.2 Preparation of composite photocatalysts

2.2.1 Preparation of N-TiO₂ photocatalysts. Tetrabutyl titanate was used as a titanium source. The dopant was ammonium chloride. First, 17 mL TBOT was dissolved in EtOH and the solution was stirred for 30 min. In the second solution, EtOH was mixed with H_2O that contained CH_3COOH .¹⁸ Then 0.6436 g NH_4Cl was added into the second solution with stirring until the dopant was dissolved. After mixing both portions, the solution was stirred to promote hydrolysis until it became transparent. The TiO_2 without dopant was prepared using the same method. The transparent solution was put into the oven at $50\text{ }^\circ\text{C}$ for 24 h and then dried at $80\text{ }^\circ\text{C}$ for several days until it became a xerogel. The dried catalysts were ground in a ball mill. The powder was collected and calcined at $500\text{ }^\circ\text{C}$ for 2 h.^{21,22}

2.2.2 Preparation of CdS/N-TiO₂. Firstly, $\text{Cd}(\text{Ac})_2 \cdot 2\text{H}_2\text{O}$ was dissolved in 60 mL distilled water, then $\text{SC}(\text{NH}_2)_2$ and $\text{NH}_3 \cdot \text{H}_2\text{O}$ were dissolved in the above solution, which was stirred for 15 min at $80\text{ }^\circ\text{C}$. Secondly, N-TiO₂ which has been prepared in the first stage was added and stirred for 22 h at $25\text{ }^\circ\text{C}$.²² Then, CdS-modified N-TiO₂ was filtrated, washed three times with 5 mL of distilled water and two times with 5 mL of acetone. Finally, the sample was dried for 3 h at ambient conditions and for 3.5 h at $110\text{ }^\circ\text{C}$. The dried catalyst was ground in a ball mill. The product was marked as CdS/N-TiO₂.

2.2.3 Preparation of CdS/N-TiO₂/ACFs. Before being used, a piece of $30 \times 75\text{ mm}$ ACF was washed with distilled water. Then, it was dried at $100\text{ }^\circ\text{C}$ for 150 min in the dry oven. Afterwards, the ACF was activated by water vapor at $800\text{ }^\circ\text{C}$ in an electric tube furnace under a N_2 atmosphere for 2 h. The composite photocatalysts were prepared as follows: first, a certain amount of epoxy resin was dissolved in acetone. Then, some photocatalysts were added into the solution with rigorous stirring for 30 min. Catalyst composites were prepared by the coupling method. Next, the ACFs were impregnated in the suspension and drawn out with a speed of 3 cm min^{-1} , then dried at $105\text{ }^\circ\text{C}$ for 4 h, so the composites could be recycled many times because of the epoxy resin's bonding effect.

2.2.4 Photochemical reaction. Powder photocatalysts and loaded photocatalysts were prepared. Both the photocatalysis experiments were performed in a batch reactor. The reactor was cylindrical with a volume of 500 mL and made of quartz glass. In this photocatalytic experiment, 500 mL MO solution was injected into the reactor and treated in the batch operation mode with a steady temperature maintained throughout the experiment in an air atmosphere. The solution was well aerated and stirred with a magnetic stirrer to ensure sufficient mixing. The dye solution was degraded in the visible light source, a 1000 W xenon lamp. For the powder photocatalysts test, the initial concentration of MO was 20 mg L^{-1} , and the catalyst was 1 g L^{-1} . Samples were taken every 5 minutes from the MO solution that had been placed under the mercury lamp. The whole UV degradation stage lasted for 180 min. In the recycling stage, the powder photocatalysts were loaded on the ACFs. A piece of loaded photocatalyst was put into the MO solution (200 mg L^{-1}). We took samples every 20 min. To determine the MO concentration, the sample solutions were subsequently measured at 462 nm. The loaded photocatalysts' reaction time for all the experiments in this work was 50 min, unless otherwise specified. For identification of the intermediate products from the MO irradiated solutions after 50 min, the sample was analyzed by a spectrometer. After one trial, the photocatalysts were washed and dried before the subsequent photocatalytic cycle test.

Characterization

The crystalline phases of the products were analyzed by X-ray diffraction (XRD), Philips X'Pert, with $\text{Cu-K}\alpha$ radiation of wavelength 0.154 nm in the range of $2\theta = 5\text{--}75^\circ$ with a scan speed of 1.2° per min. The morphology and size of the photocatalytic nanoparticles and the element content were observed by an S-4800 field emission scanning electron microscopy (SEM and SEM-EDS Hitachi, Japan). The high resolution microstructure was studied by transmission electron microscopy (TEM, Gatan ORIOUSTM SC200C-CD). A UV-Vis spectrometer (UV-3100, Shanghai, China) was used to identify the band shift in the range of 190 to 1000 nm. The light corrosion degree was calculated by AAS (Atomic Spectroscopy Absorption) using an analysis system (ContraAA 700, Analytik Jena). The BET surface area, pore volume and pore size of the photocatalysts were obtained by N_2 adsorption using a BET specific surface area analyzer (ASAP2020, micrometrics, USA).

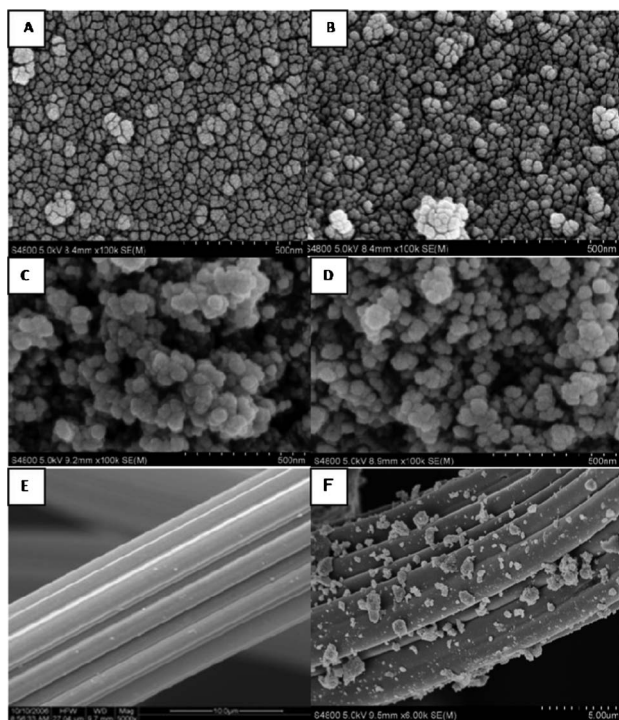


Fig. 1 The morphology and structure of the N-doped and CdS-coupled TiO_2 nanocomposites and the original ACF_0 , $\text{CdS/N-TiO}_2/\text{ACFs}$. (A) Bare TiO_2 , (B) N-TiO_2 , (C) CdS/TiO_2 , (D) CdS/N-TiO_2 , (E) original ACF_0 , (F) $\text{CdS/N-TiO}_2/\text{ACFs}$.

The concentration of MO was measured by a supernatant spectrometer (UV-3100, Shanghai, China).

Results and discussion

Structure characterization

The microstructural characterization of the nanocomposites was carried out by scanning electron microscopy (SEM). Fig. 1 and Fig. 2 show the SEM images and SEM-EDS (Energy

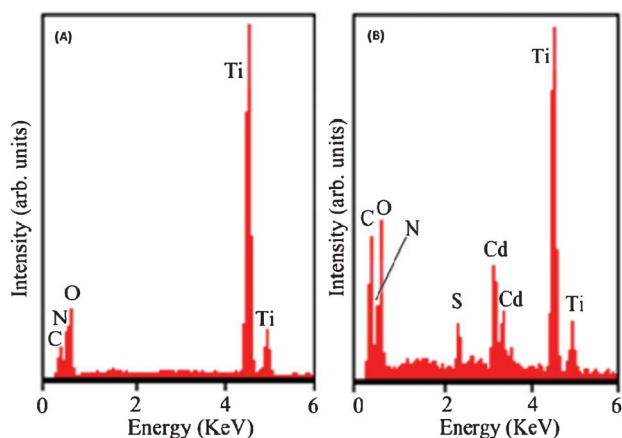


Fig. 2 SEM-EDS spectrum of (A) N-TiO_2 , (B) CdS/N-TiO_2 nanocomposites.

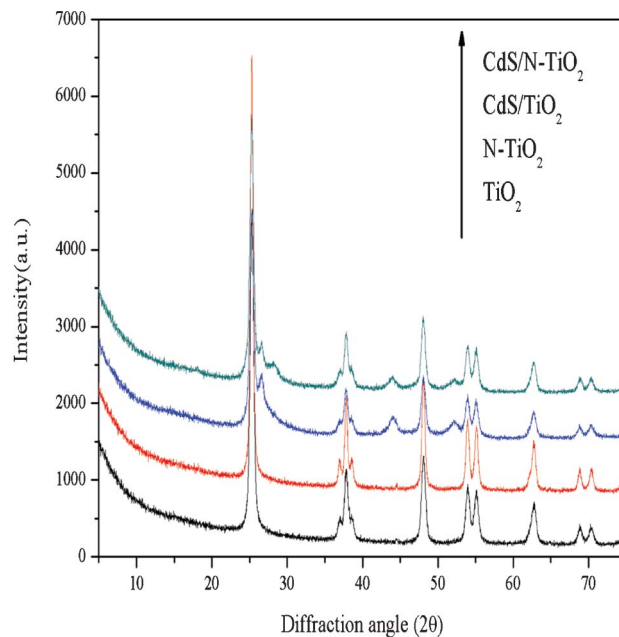


Fig. 3 XRD spectra measured for bare TiO_2 , N-TiO_2 , CdS/TiO_2 , CdS/N-TiO_2 .

Dispersive Spectrometer) spectra of the structure of the CdS-coupled TiO_2 nanocomposite. The SEM images (Fig. 1) show that N-doped TiO_2 represent stacked nanoparticles with a diameter of 18 ± 2 nm and particle size increased after being coupled with CdS to 27–30 nm approximately. It was clear that those nanoparticles maintained their original crystalline structure, but their size visibly increased due to conglomeration. The EDS profile showed correct stoichiometry of CdS to TiO_2 in the nanocomposite structure. The atomic ratio of N, S, Cd and Ti in the nanocomposite structure was 12 : 1 : 2 : 8 at.% obtained from the SEM-EDS spectrum as shown in Fig. 2. Cd and S atoms did not reach the theoretical ratio of 1 : 1, which may be caused by S atoms being doped into the interior of the catalysts, or the decrease of S atoms on the surface of the photocatalyst.

The X-ray diffraction, as shown in Fig. 3, was used to determine the phase composition of the samples' weight fraction of each phase and crystallite size. The diffraction peaks at $2\theta = 25.3^\circ$, 37.8° , 54.0° can be attributed to anatase- TiO_2 . The diffraction peaks at 26.5° , 44.1° , 52.1° which could be assigned to the CdS cubic phase were also observed. The peak intensity of anatase increased and the width of the anatase phase became narrower after doping with N, which suggested that the particle size increased. After loading the CdS nanoparticles, the XRD (Fig. 3) patterns displayed rather weak CdS peaks which might result from the high dispersion of CdS and the low content of loaded CdS. This indicated that there was no significant change of the TiO_2 substrate with high crystallinity during the loading process. The average particle size was estimated from the crystal size by applying Scherrer's formula on anatase (101) and (111) diffraction from XRD. The average size of CdS/TiO_2 and CdS/N-TiO_2 was 24 nm and 27 nm respectively. A deeper insight into the fine structure showed that different patterns of nanoparticles studied by

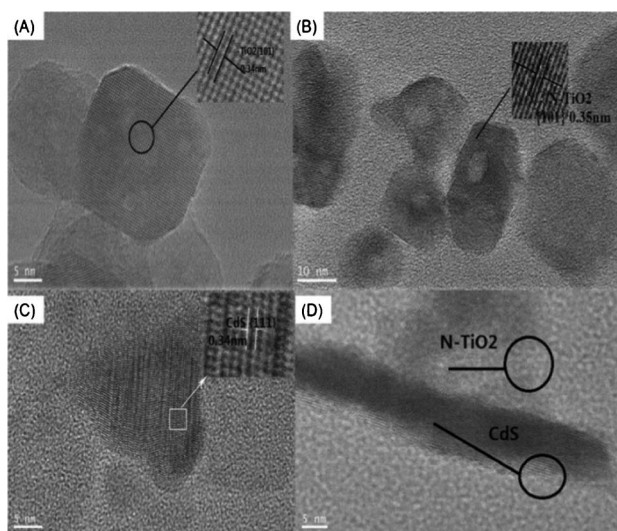


Fig. 4 TEM images for different kinds of TiO_2 : (A) pure TiO_2 , (B) N-TiO_2 , (C) CdS/TiO_2 , (D) CdS/N-TiO_2 .

TEM (Fig. 4) revealed that the nanoparticles were undoubtedly loaded onto the surface of TiO_2 and the crystalline structure of TiO_2 was not influenced by the deposition of CdS . The lattice space of CdS was 0.34 nm, which corresponds to the (111) plane of cubic CdS and that of N-TiO_2 was 0.35 nm, which matched the (101) plane of anatase.

The photocatalyst had an increase in the total pore volume and average pore diameter after being doped and coupled, while having a slight decrease in the BET surface area, as shown in Table 1. Table 2 shows that the BET surface area of ACF *via* activation by vapor had an obvious decrease from $1198 \text{ m}^2 \text{ g}^{-1}$ to $1676 \text{ m}^2 \text{ g}^{-1}$. The porous structure of ACF was significantly altered after loading with the photocatalyst. The specific surface area was reduced from $1676 \text{ m}^2 \text{ g}^{-1}$ to $1101 \text{ m}^2 \text{ g}^{-1}$ and the total volume also had a slight decrease from $0.6959 \text{ cm}^3 \text{ g}^{-1}$ to $0.5453 \text{ cm}^3 \text{ g}^{-1}$ indicating that the ACF were remarkably blocked by the loaded photocatalyst. The increase of the average pore diameter of ACF was attributed to the activation by vapor at $800 \text{ }^\circ\text{C}$. The coating of the nanoscale photocatalyst was basically distributed evenly on the outer surface of the fiber with scattered aggregates of the photocatalyst. Although the photocatalysts had been on the deposited surface of ACF as was shown in Fig. 1-(F) and some had blocked micropores, the photocatalysts' system retained the same spatial distribution of carbon fibers as in their unsupported state, allowing the light to penetrate into the photocatalysts.

Table 1 Microstructures of pure TiO_2 , N-TiO_2 , CdS/TiO_2 , CdS/N-TiO_2

	Samples			
	TiO_2	N-TiO_2	CdS/TiO_2	CdS/N-TiO_2
BET surface area ($\text{m}^2 \text{ g}^{-1}$)	65.8762	68.9720	40.4567	48.4292
Total pore volume ($\text{cm}^3 \text{ g}^{-1}$)	0.2030	0.2777	0.2741	0.4067
Average pore diameter (nm)	12.3270	16.1059	27.1056	33.5926

Table 2 Microstructures of original ACF_0 , ACF, $\text{CdS/N-TiO}_2/\text{ACF}$

	Samples		
	ACF_0	ACF	$\text{CdS/N-TiO}_2/\text{ACF}$
BET surface area ($\text{m}^2 \text{ g}^{-1}$)	1198	1676	1101
Total pore volume ($\text{cm}^3 \text{ g}^{-1}$)	0.4866	0.6959	0.5453
Average pore diameter (nm)	1.6247	1.6608	1.9811

Photophysical properties

The photodegradation of MO was used as a probe to evaluate the performance of the photocatalysts. According to the dependence of the photodegradation rate on the reaction time (Fig. 5), the photodegradation of 20 mg L^{-1} MO with N-TiO_2 , CdS/TiO_2 and CdS/N-TiO_2 was completed within 180 min. The photodegradation efficiency of MO with the CdS/N-TiO_2 composites was obviously higher than the other three kinds of photocatalysts and the MO solution was completely decomposed after 80 min irradiation, as shown in Fig. 5. This result demonstrated that the introduction of CdS and N could significantly extend the light absorbance into the visible light region and thus promote the photocatalytic activity under visible light irradiation. When irradiated for 40 min under visible light, the degradation rate of MO with CdS/N-TiO_2 was about 200% higher than that of pure TiO_2 . Generally, the activity of a photocatalyst is also affected by many factors such as surface area, phase area, phase structure and crystallinity. Although the N-doping process induced a slight increase in the BET surface area (Table 1), the BET surface area decreased after coupling with CdS . The obtained samples exhibited greatly enhanced photocatalytic properties. This indicated that the texture properties of the modified TiO_2 were not the crucial factor affecting the photocatalytic properties. Bare TiO_2 could

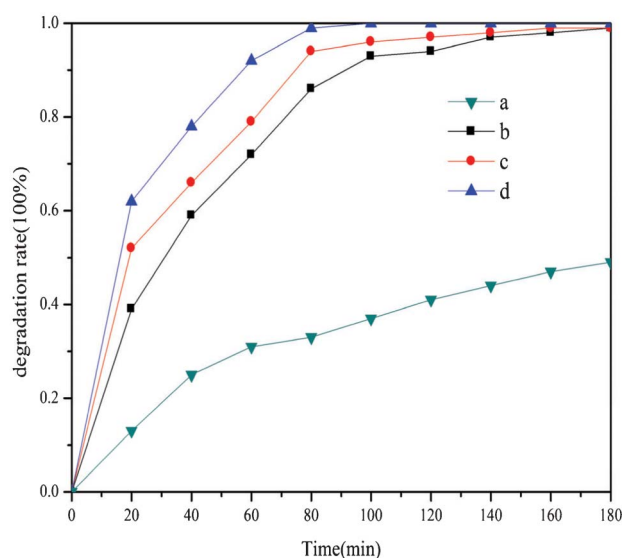


Fig. 5 Effect of photocatalyst on the degradation rate of MO for (a) pure TiO_2 , (b) N-TiO_2 , (c) CdS/TiO_2 , (d) CdS/N-TiO_2 , under visible light, with initial MO concentration = 20 mg L^{-1} .

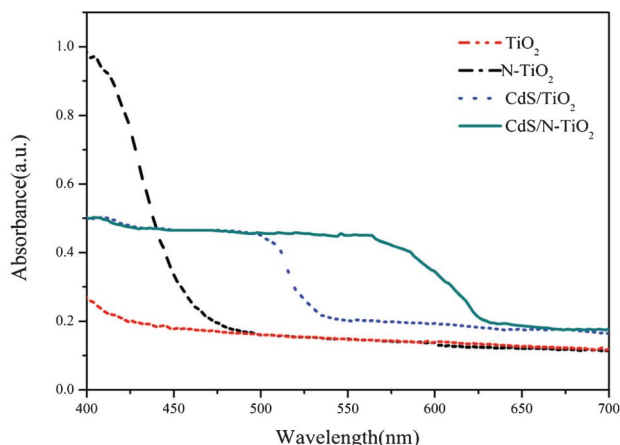
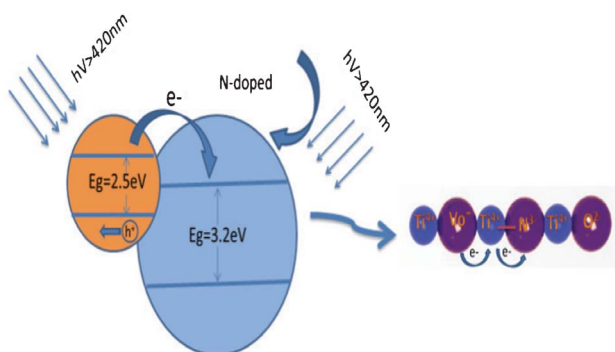


Fig. 6 UV-Visible absorbance spectra of TiO_2 , N-TiO_2 , CdS/TiO_2 , CdS/N-TiO_2 .

only absorb UV light with wavelengths less than 400 nm because of the large energy gap of anatase. The absorption centre of N-TiO_2 is at around 430 nm. The introduction of CdS and N could efficiently enhance the absorption range of TiO_2 . Shifts in the absorbance spectra of the other three kinds of photocatalysts toward the visible light region were observed in the UV-Vis absorbance spectra (Fig. 6). The N-doped TiO_2 , calcined at 500 °C, had increased intensity at both the absorption center at 430 nm and the tail absorption above 500 nm, while the absorption edge was red-shifted to 630 nm after being doped and coupled (CdS/N-TiO_2). As we know, the efficient charge transfer from CdS to the N-TiO_2 conduction band could effectively separate photo-induced electrons from holes in the CdS and thus inhibit their recombination, resulting in the enhanced charge density in TiO_2 (Scheme 1), because for n-type semiconductors the charge transfer is dominated by the majority carrier, *i.e.* the electrons. The nitrogen doping could narrow the band gap of titania from 3.20 eV to 2.85 eV in our work, which could be estimated from the plot of the square root of Kubelka–Munk function $F(R)$ versus photon energy.²³ This narrower band gap would facilitate the excitation of electrons from the valence band to the conduction band in the doped oxide semiconductor under visible light illumination, which can result in higher photo-

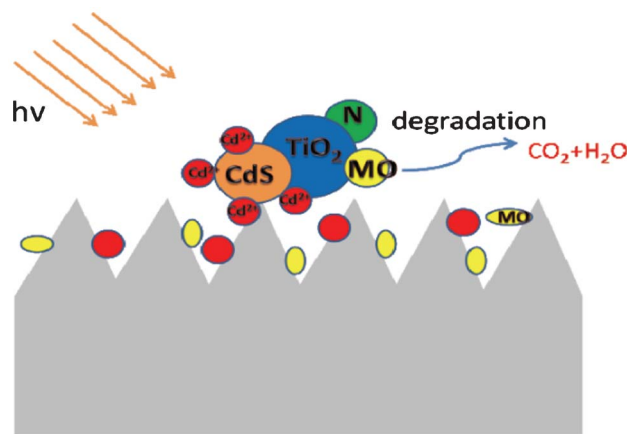


Scheme 1 Illustration of electron transfer in the CdS/N-TiO_2 composite.

catalytic activities. Furthermore, N-doped TiO_2 contains an oxygen vacancy and surface $[\text{Ti}^{4+}-\text{N}^{3-}]$ unit states.²⁴ A synergistic effect of N dopant and oxygen vacancy in TiO_2 contributed to the great enhancement of the visible light photoactivity. The lower recombination of the photocatalyst indicated that electrons and holes in CdS/N-TiO_2 led to improved efficiency and facilitated the formation of active radicals which decomposed organic compounds. Also, in the photocatalytic systems where both electrons and holes should transfer concurrently to maintain the electroneutrality condition, the activities of photoreduction were coupled with those of photooxidation. The excellent photocatalytic performance is attributed to four aspects: (i) low band gap energy, (ii) fast electron transfer, (iii) open mesoporous structure with large surface area, (vi) N-doped TiO_2 containing an oxygen vacancy and surface $[\text{Ti}^{4+}-\text{N}^{3-}]$ unit.²³ Among them, the benefits of the substrates were the formation of an open mesoporous architecture with large surface area that would not only provide more active sites for reaction molecules, but also supply effective transport paths for both reactant and product molecules in chemical reactions.^{25,26} Besides, the larger surface area enhanced the light harvesting and effectively promoted the separation efficiency of the electron–hole pairs. So the above different performances of photocatalysts, using both N-doped and CdS-coupled TiO_2 had better photocatalytic properties.

Leaching studies

In an attempt to prevent the Cd^{2+} ions from leaching, the photocatalysts were supported on activated ACFs, as shown in Scheme 2. When the photocatalysts were loaded on the ACFs, first, the pollutant, MO, was absorbed on absorbent supports, resulting in a higher pollutant environment around the loaded composites, then the absorbed MO molecules were transferred to the catalysts by diffusion and decomposed there, and Cd^{2+} ions were produced at the same time because of the photocorrosion. The ACFs could absorb most of the Cd^{2+} .²⁷ The tendency of $\text{CdS/N-TiO}_2/\text{ACFs}$ and CdS/N-TiO_2 to leach out Cd^{2+} ions under photodegradation in the visible region



Scheme 2 Illustration of the photocatalytic activity of the $\text{CdS/N-TiO}_2/\text{ACF}$ system under visible light.

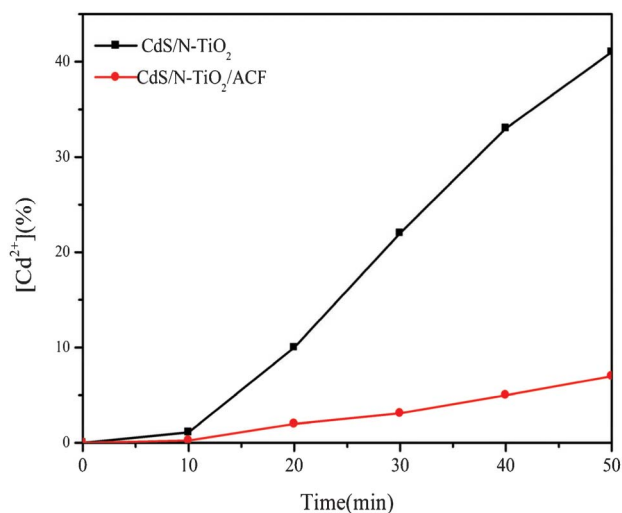


Fig. 7 Reaction profiles showing the concentration (%) of Cd²⁺ ions leaching out of CdS/N-TiO₂ and CdS/N-TiO₂/ACF under visible light with 200 mg L⁻¹.

was also studied. CdS/N-TiO₂/ACFs made a significant difference, as shown in Fig. 7. Leaching occurred from both composites, but the amount of leaching from CdS/N-TiO₂/ACFs is obviously lower due to the adsorptive capacity of ACFs. The percentage values of Cd²⁺ leaching after 60 min were 38% and 7%, respectively. Therefore, the decrease in the photoactivity of CdS/TiO₂ described above could be mainly attributed to the loss of CdS, which may be the origin of the low stability of the catalysts. Meanwhile, it is worth noting that the ACFs presented a strong link between CdS and TiO₂, which promoted stable photoactivity.

Catalyst recovery and reuse

The CdS sensitized mesoporous N-TiO₂ loaded on the ACFs by the coupling method exhibited good activity and high stability. To evaluate the stability of the loaded photocatalysts, we carried out recycling degradation tests on CdS/N-TiO₂/ACF, CdS/TiO₂/ACF, and ACF. Activated ACFs had larger BET areas than the original samples. In order to test the feasibility of reusing the different kinds of composite photocatalysts, three degradation cycles of MO were carried out as shown in Fig. 8. The degradation percentage of MO after three cycles, indicated that the photocatalytic activity of CdS/N-TiO₂/ACFs slightly decreased after 30 min of irradiation, from 100% in the first circle to 87% in the third circle due to the photocorrosion of CdS. It appeared that the deposited photocatalysts had firmly attached onto the active carbon fiber surface, as observed from SEM images (Fig. 1). At the same time, it was also proved that the final removal of MO from the solutions was caused by photocatalytic degradation rather than absorption. These results indicated the cyclic usage of ACFs with satisfactory stability in the polluted water. However, loading on the ACFs could not reduce the photocorrosion of CdS, but prevented the leaching of Cd²⁺. Furthermore, the decrease of leaching out of Cd²⁺ in the test might also be mainly caused by the forces between CdS and TiO₂, which had a positive influence on the CdS/N-TiO₂ stability.

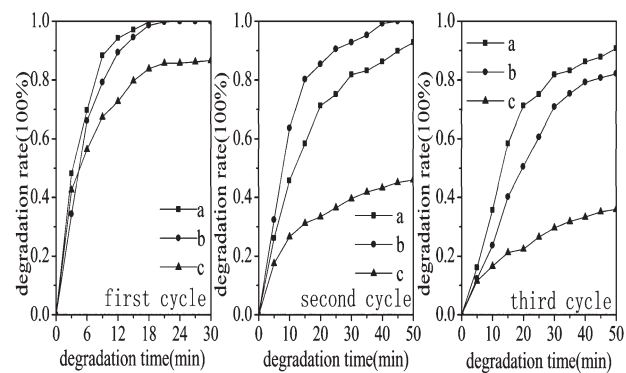


Fig. 8 Effect of photocatalyst on the degradation efficiency of MO for (a) CdS/N-TiO₂/ACF, (b) CdS/TiO₂/ACF, (c) ACF, with time, under visible light, with initial MO concentration = 200 mg L⁻¹.

Conclusions

The nanostructure and composition of a semiconductor through coupling and doping can be designed for higher solar conversion efficiency. In this work, CdS/N-TiO₂ was successfully synthesized and tested for its photocatalytic activity. CdS/N-TiO₂ exhibited much higher photocatalytic activity than N-TiO₂ and CdS/TiO₂ under visible light. The result showed that the semiconductor coupling and N-doping modifications have a synergistic effect on enhancing the photocatalytic performance based on two facts: first, the charge-transfer process between CdS and TiO₂ resulting in the effective physical separation of photogenerated electrons and holes;^{28,29} second, the N-doped TiO₂ containing an oxygen vacancy and surface [Ti⁴⁺-N³⁻] unit.²⁴ Loading the photocatalysts onto ACFs can prevent Cd²⁺ leaching efficiently, which has a positive influence on the CdS/N-TiO₂ stability. However, the mechanism of CdS and N dopant on the photocatalytic activity needs to be further investigated.

Acknowledgements

This work is financially supported by the National Natural Science Foundation of China (Grant No. 20776159 and 51202294), the Fundamental Research Funds for the Central Universities (09CX05009A), Natural Science Foundation of Shandong province (No. ZR2009FL028) and National Basic Research Program of China (NO. 2011CB605703).

Notes and references

- 1 A. Fujishima and K. Honda, *Nature*, 1972, **238**, 37–38.
- 2 J. Senthilnathan and L. Philip, *Chem. Eng. J.*, 2011, **172**, 678–688.
- 3 S. Giraudet, P. Pré, H. Tezel and P. Le Cloirec, *Carbon*, 2006, **44**, 2413–2421.

- 4 D. Di Valentin, E. Finazzi, G. Pacchioni, A. Selloni, S. Livraghi, M. C. Paganini and E. Giamiello, *Chem. Phys.*, 2007, **339**, 44–56.
- 5 H. Kisch, S. Sakthivel, M. Janczarek and D. Mitoro, *J. Phys. Chem. C*, 2007, **111**, 11445–11449.
- 6 S. Shanmugasundaram and K. Horst, *Angew. Chem., Int. Ed.*, 2003, **42**, 4908–4911.
- 7 R. Asahi, T. Morikawa, T. Ohwaki, K. Aoki and Y. Taga, *Science*, 2001, **293**, 269–271.
- 8 Y. Bessekhoud, N. Chaoui, M. Trzpit, N. Ghazzal, D. Robert and J. V. Weber, *J. Photochem. Photobiol., A*, 2006, **183**, 218.
- 9 K. Demeestere, J. Dewulf, T. Ohno, P. H. Salgado and H. V. Langenhove, *Appl. Catal., B*, 2005, **61**, 140.
- 10 J. C. Trista, F. Magalhaes, P. Corio and M. T. C. Sansiviero, *J. Photochem. Photobiol., A*, 2006, **181**, 152.
- 11 L. Wu, J. C. Yu and X. Z. Fu, *J. Mol. Catal. A: Chem.*, 2006, **244**, 25.
- 12 L. Wan and J. Y. Feng, *Res. Environ. Sci.*, 2009, **22**, 95.
- 13 Q. Zhang, J. Su, X. H. Zhang, J. Li, A. Q. Zhang and Y. H. Gao, *New J. Chem.*, 2012, **36**, 2302–2307.
- 14 Z. Ding, X. J. Hu, P. L. Yue, G. Q. Lua and P. F. Greenfield, *Catal. Today*, 2001, **68**, 173.
- 15 Y. M. Xu, W. Zheng and W. P. Liu, *J. Photochem. Photobiol., A*, 1999, **122**, 57.
- 16 A. Bhattacharyya, S. Kawi and M. B. Ray, *Catal. Today*, 2004, **98**, 431.
- 17 W. H. Leng, H. Liu, S. A. Cheng, J. Q. Zhang and C. N. Cao, *J. Photochem. Photobiol., A*, 2000, **131**, 125.
- 18 P. A. Deveau, F. Arsac, P. X. Thivel, C. Ferronato, F. Delpech, J. M. Chovelon, P. Kaluzny and C. Monnet, *J. Hazard. Mater.*, 2007, **144**, 692–697.
- 19 J. Shi, J. Zheng and P. Wu, *Catal. Commun.*, 2008, **9**, 1846–1850.
- 20 H. H. Ou and S. L. Lo, *J. Hazard. Mater.*, 2007, **146**, 302–308.
- 21 D. Li, H. Haneda, S. Hishita and N. Ohashi, *Mater. Sci. Eng., B*, 2005, **117**, 67–75.
- 22 F. Peng, L. Cai, H. Yu, H. Wang and J. Yang, *J. Solid State Chem.*, 2008, **181**, 130–136.
- 23 R. Asahi, T. Morikawa, T. Ohwaki, A. Aoki and Y. Yaga, *Science*, 2001, **293**, 269–271.
- 24 W. X. Zhao, Z. P. Bai, A. Ren, B. Guo and C. Wua, *Appl. Surf. Sci.*, 2010, **256**, 3493–3498.
- 25 Z. Z. Zhang, X. X. Wang and J. L. Long, *J. Catal.*, 2010, **276**, 201–214.
- 26 G. S. Li, D. Q. Zhang and J. C. Yu, *Environ. Sci. Technol.*, 2009, **43**, 7079–7085.
- 27 A. T. Bell, *Science*, 2003, **299**, 1688–1691.
- 28 J. W. Tang, Z. G. Zou and J. H. Ye, *Chem. Mater.*, 2004, **16**, 1644–1649.
- 29 M. Anpo and M. Takeuchi, *J. Catal.*, 2003, **216**, 505.